

High-precision mass measurements of nickel, copper, and gallium isotopes and the purported shell closure at $N=40$

C. Guénaut,^{1,*} G. Audi,¹ D. Beck,² K. Blaum,^{2,3} G. Bollen,⁴ P. Delahaye,⁵ F. Herfurth,²
A. Kellerbauer^{†,5} H.-J. Kluge,^{2,6} J. Libert,⁷ D. Lunney,¹ S. Schwarz,⁴ L. Schweikhard,⁸ and C. Yazidjian²

¹*CSNSM-IN2P3-CNRS, 91405 Orsay-Campus, France*

²*GSI, Planckstraße 1, 64291 Darmstadt, Germany*

³*Johannes Gutenberg-Universität, Institut für Physik, 55099 Mainz, Germany*

⁴*NSCL, Michigan State University, East Lansing, MI 48824, USA*

⁵*CERN, Physics Department, 1211 Genève 23, Switzerland*

⁶*Physikalisches Institut, Universität Heidelberg, 69120 Heidelberg, Germany*

⁷*Institut de Physique Nucléaire, IN2P3-CNRS, 91406 Orsay-Campus, France*

⁸*Institut für Physik, Ernst-Moritz-Arndt-Universität, 17487 Greifswald, Germany*

(Dated: January 23, 2007)

High-precision mass measurements of more than thirty neutron-rich nuclides around the $Z=28$ closed proton shell were performed with the triple-trap mass spectrometer ISOLTRAP at ISOLDE/CERN to address the question of a possible neutron shell closure at $N=40$. The results, for $^{57,60,64-69}\text{Ni}$ ($Z=28$), $^{65-74,76}\text{Cu}$ ($Z=29$), and $^{63-65,68-78}\text{Ga}$ ($Z=31$), have a relative uncertainty of the order of 10^{-8} . In particular, the masses of $^{72-74,76}\text{Cu}$ have been measured for the first time. We analyse the resulting mass surface for signs of magicity, comparing the behavior of $N=40$ to that of known magic numbers and to mid-shell behavior. Contrary to nuclear spectroscopy studies, no indications of a shell or sub-shell closure are found for $N=40$.

PACS numbers: 21.10.Dr, 21.60.Cs, 27.50.+e, 32.10.Bi

I. INTRODUCTION

A striking parallel between the atomic and nuclear systems is the occurrence of closed shells. The behavior of the atomic system is largely governed by what can be considered as an infinitely massive and point-like nucleus. Describing nuclear behavior, however, is a particularly difficult task given its composition of neutrons and protons, similar in mass yet different in charge. The nucleon interaction is so complicated that ground-state properties are not globally predicted with particularly good precision. A property crucial to the understanding of the nuclear system is the behavior of its shell structure as a function of the varying composition of protons and neutrons. The fact that shell structure seems to be modified in systems where the number of neutrons N and the number of protons Z are unbalanced (*i.e.* far from the equilibrium region of stable nuclides) is one of the key questions of today's nuclear physics research.

Over the last 20 years, magic numbers have been found to vanish in certain region of the chart of nuclides, the first one being $N=20$ for sodium [1] and later, magnesium [2]. More recently, $N=8$ [3, 4] and $N=28$ [5, 6] have also disappeared. Conversely, “new” magic numbers such as $N=16$ [3] and $N=32$ [7, 8, 9] have also been

found. One case of particular interest is that of $N=40$ because of the unexpected events that have transpired since the first studies in 1982. At that time, Bernas *et al.* [10] showed that the first excited state of $^{68}\text{Ni}_{40}$ was 0^+ , establishing a new case of 2^+ and 0^+ inversion. This was compared to the case of $^{40}\text{Ca}_{20}$, a doubly-magic nuclide [11] where such an inversion was known. Consequently, Bernas *et al.* concluded ^{68}Ni to be doubly-magic.

In 1995, Broda *et al.* [12] published a comprehensive summary of spectroscopy work since 1982 and elaborated the excited spectrum of ^{68}Ni , finding the first excited state to be 0^+ (as Bernas *et al.* [10]), 2^+ as the second excited state and a 5^- isomeric state. As this is the same situation for the ^{80}Zr excited states, they concluded that ^{68}Ni was spherical, implying a significant sub-shell closure at $N=40$. Shell-model predictions of isomeric states near magic nuclides motivated the experimental investigations of Grzywacz *et al.* [13] in 1998. They discovered many isomeric states in the vicinity of ^{68}Ni , further strengthening the case for its doubly-magic character. In 1999, β -decay studies were carried out by Hannawald *et al.* [14], who found long half-lives for the neighboring isotones (copper, manganese) at $N=40$ indicating an increase in collectivity. However, β -decay studies by Mueller *et al.* [15] the same year showed that the stabilizing effect of $N=40$ disappeared when moving away from ^{68}Ni .

The powerful tool of Coulomb excitation was brought to bear on ^{68}Ni in 2002 when Sorlin *et al.* [16] measured the $B(E2)$ value (which is the probability of transition between the ground state 0^+ and the excited state 2^+). $B(E2)$ is expected to be small for magic nuclides which are difficult to excite, and to be large for deformed nu-

[†]Present address: Max Planck Institut für Kernphysik, Postfach 103980, 69029 Heidelberg, Germany

*Corresponding author; Present address: NSCL, Michigan State University, East Lansing, MI 48824, USA; E-mail address: guenaut@nscl.msu.edu

clides. The measured $B(E2)$ value was unexpectedly small, reinforcing the magic nature of ^{68}Ni . Sorlin *et al.* attributed the lack of corroborating evidence from the mass surface to an erosion of the $N = 40$ sub-shell, erosion confirmed by recent measurements [17, 18]. However, a concerted theoretical effort published by Langanke *et al.* [19] argued against the doubly-magic nature of ^{68}Ni , noting that the “missing” $B(E2)$ strength lies at much higher energy (>4 MeV).

According to Bohr and Mottelson [20]: “In terms of the expansion of the total binding energy, the shell structure appears as a small correction compared to the surface energy... Despite the smallness of these effects on the scale of the total nuclear energy, they are of decisive importance for the structure of the low-energy nuclear spectra...” In the light of these conflicting experimental and theoretical signatures as well as the relatively large uncertainty on the binding energies in this interesting region, high-precision mass measurements were carried out with the mass spectrometer ISOLTRAP in an attempt to bring some clarification to this situation. Time-of-flight mass measurements had been performed in 1994 [21] but although they gave no indication that $N = 40$ was magic, the precision was insufficient to be conclusive. The most accurate mass measurements today are performed in Penning traps [22, 23] and ISOLTRAP at CERN has pioneered the application to radioactive nuclides [24, 25]. The experimental setup of ISOLTRAP is presented in section II, and the measurements in the region of $N = 40$ and their evaluation are described in section III. A comparison to mass models follows in section IV and the question of $N = 40$ is discussed in the light of the new results in the last section.

II. THE ISOLTRAP SETUP

A. Experimental setup

ISOLTRAP is a high-precision Penning-trap mass spectrometer, located at CERN’s ISOLDE facility [26] which delivers mass-separated beams of radionuclides. ISOLTRAP is composed of three main parts (see Fig. 1). First, a linear gas-filled radio-frequency quadrupole (RFQ) trap, used as cooler and buncher, adapts the 60-keV ISOLDE ion beam to the ISOLTRAP requirements with respect to kinetic energy, time structure, and beam emittance [27]. The second part is a gas-filled, cylindrical Penning trap [28] in which a mass-selective helium buffer-gas cooling technique [29] with a resolving power of up to 10^5 is used for isobaric cleaning. This preparation trap is installed in a $B=4.7$ T superconducting magnet. Finally, the cooled ion bunch is transferred to the precision Penning trap for isomeric separation (when required) and mass measurement. The precision Penning trap is installed in a second superconducting magnet ($B=5.9$ T). The mass is determined by measuring the true cyclotron frequency $\nu_c = qB/(2\pi m)$ of the stored ion (see next

paragraph). The magnetic field B is determined from a measurement of the cyclotron frequency of a reference ion whose mass is well known. The setup also includes an off-line ion source to produce stable ions, used as reference masses.

B. Mass measurement procedure

Ion confinement in a Penning trap is based on the application of an electrostatic field and a magnetic field to store ions in the axial and radial directions, respectively. The ion motion in a Penning trap is a superposition of three independent harmonic oscillator modes, one in the axial direction with frequency ν_z and two in the radial direction, *i.e.* the cyclotron motion with reduced frequency ν_+ , and the magnetron motion with frequency ν_- [30, 31]. In a purely quadrupolar electric field, the frequencies are related as follows:

$$\nu_c = \nu_+ + \nu_- \quad (1)$$

Ion beams are alternatively delivered from ISOLDE or from an off-line ion source and injected into the RFQ, mounted on a 60-keV pedestal, where they are cooled and bunched. The ion bunch from the RFQ is sent to the preparation trap. Ion collisions with the buffer gas inside this trap first cool the axial motion. A dipolar excitation with a frequency ν_- is then applied to increase the magnetron radius of all ion species, making it larger than the exit hole of the trap. To select the ions of interest, an azimuthal quadrupole radio-frequency electric field at frequency ν_c is applied which couples the radial modes. Since one mode is cooled by the gas, the radius is reduced and the ion cloud is centered. In this way the trap works as an isobar separator with a resolving power $R = m/\Delta m$ of 10^4 to 10^5 [28].

The purified ion beam is transferred to the precision trap, where different excitations are performed. A phase-sensitive dipolar excitation at ν_- is applied to increase the magnetron radius of the ion motion [32]. If there are contaminants (isobars or isomers), a second, mass-dependent dipolar excitation is performed at ν_+ to remove them [33]. Finally, an azimuthal quadrupole radio-frequency field is applied to convert the initial magnetron motion into cyclotron motion. At $\nu_{RF} = \nu_c$, a full conversion is obtained, leading to an increase of the orbital magnetic moment μ and the associated radial kinetic energy $E = \mu B$ [34]. After ejection at low axial energy, ions pass the inhomogeneous part of the magnetic field on their way to an MCP detector (recently replaced by a channeltron detector [35]) at the top of the setup. Since the axial acceleration in this fringe field is proportional to $\mu \cdot \partial B/\partial z$, the shortest time of flight (TOF) is observed for $\nu_{RF} = \nu_c$ [36].

The mass resolution in the precision trap depends strongly on the conversion time used for the excitation. The line width $\Delta\nu$ of the resonance is mainly determined

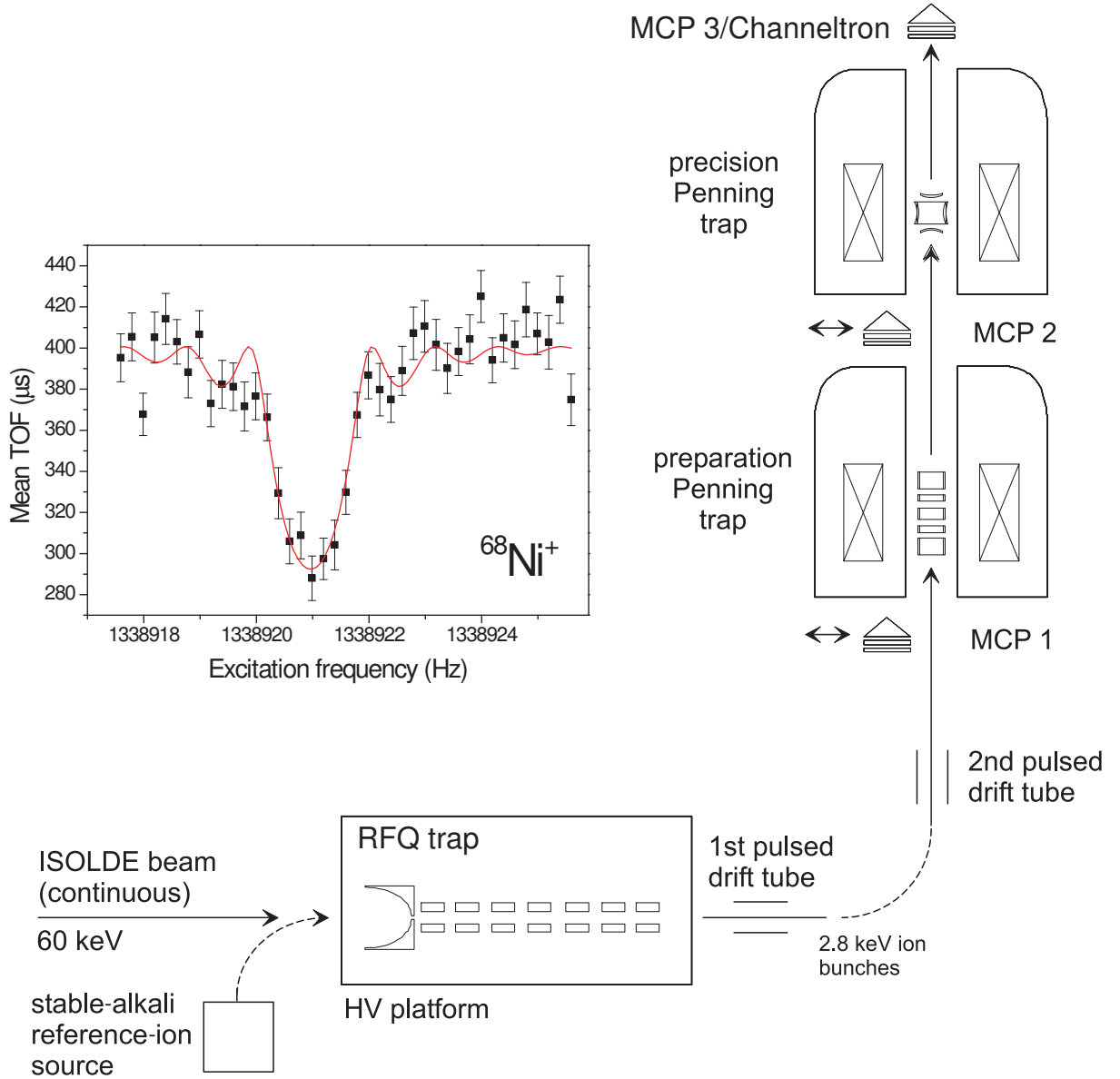


FIG. 1: Sketch of the experimental setup of the ISOLTRAP mass spectrometer, including the main parts: a gas-filled linear radio-frequency quadrupole (RFQ) trap for capturing and preparing the ISOLDE beam, a gas-filled cylindrical Penning trap for isobaric separation, and a hyperbolic Penning trap for the mass measurement. The micro-channel plate (MCP) detectors are used to monitor the ion transfer and to measure the extracted-ion time of flight (TOF) together with the channeltron detector. The inset presents a time-of-flight (TOF) cyclotron resonance for radioactive $^{68}\text{Ni}^+$ ions.

by the duration of the applied RF-field (T_{RF}) used to couple the two radial motions. The relation is [34]:

$$\Delta\nu(FWHM) \approx \frac{0.9}{T_{RF}}. \quad (2)$$

The statistical precision in the cyclotron frequency determination is given by [37]:

$$\frac{\delta\nu}{\nu} \propto \frac{1}{\nu T_{RF} \sqrt{N}}, \quad (3)$$

with N being the number of ions and $R = \nu T_{RF}$ the re-

solving power. With sufficiently long excitation times (few seconds), a resolving power of up to 10^7 can be reached. As an example of a cyclotron frequency measurement, the inset of Fig.1 presents the time-of-flight (TOF)-resonance curve of one of the two measurements of radioactive ^{68}Ni . The mean TOF of the ions as a function of the applied radio-frequency (RF) is shown. The solid line is a fit of the well-known line-shape [31] to the data points. This measurement was performed with about 1000 ions using an excitation time $T_{RF} = 900$ ms, resulting in a resolving power of 1.1×10^6 and a relative

frequency uncertainty of $\delta\nu/\nu = 6 \times 10^{-8}$.

III. MEASUREMENTS OF THE NI, CU, AND GA ISOTOPES

The nuclides $^{57,60,64-69}\text{Ni}$, $^{65-74,76}\text{Cu}$, and $^{63-65,68-78}\text{Ga}$ have been investigated with ISOLTRAP. They were produced at ISOLDE by bombarding a uranium carbide (UC) target with 1.4-GeV protons from CERN's Proton Synchrotron Booster. The ionization was achieved for gallium with a tungsten (W) surface ionization ion source and for copper and nickel with the resonance ionization laser ion-source (RILIS) [38]. ISOLDE's General Purpose Separator (GPS), with a mass resolving power of about 1000 was used. The proton-rich isotopes $^{63-65}\text{Ga}$ were measured in a different experiment using a ZrO target and ISOLDE's High Resolution Separator (HRS), which has a mass-resolving power of about 3000. Both targets were bombarded using pulses containing up to 3×10^{13} protons.

The yields of nickel and copper were fairly intense at about 10^5 ions/s. The efficiency of ISOLTRAP is better than 1% so a beam gate was used in order to limit the number of ions sent to the precision trap and minimize ion-ion interactions that cause frequency shifts. The typical number of ions simultaneously stored in the precision trap was between 1 and 8.

Despite the good yields of nickel and copper nuclides, up to three orders of magnitude more surface-ionized gallium was present. For the measurement of ^{68}Ni shown in Fig. 1, a cleaning of ^{68}Ga was applied in the preparation trap. The ratio between the yield of ^{68}Ga and ^{68}Ni was “only” a factor of ten which was low enough to allow an effective cleaning. This ratio was higher farther from stability and prevented the measurement of more neutron-rich nickel and copper since the preparation trap was saturated by the gallium isobars. Similarly, a significant contamination of titanium oxide prevented the measurement of more proton-rich gallium isotopes, and the presence of rubidium isobars made the measurement of more neutron-rich gallium isotopes impossible.

The results from the data analysis is the ratio $\nu_{c,ref}/\nu_c$ [39], since the atomic mass m of the ions is calculated from the ratio between the cyclotron frequency of the reference ion $\nu_{c,ref}$ and the cyclotron frequency of the ion of interest ν_c , the atomic mass of the reference ^{85}Rb [40], and the electron mass m_e :

$$m = \frac{\nu_{c,ref}}{\nu_c} (m_{^{85}\text{Rb}} - m_e) + m_e. \quad (4)$$

All the results were evaluated in order to include them in the Atomic-Mass Evaluation (AME) table [41]. The table of atomic masses results from an evaluation of all available experimental data on masses, including direct measurements as well as decay and reaction studies. The AME forms a linked network and uses a least-squares adjustment to derive the atomic masses. Among all nuclear

ground-state properties, such an evaluation is unique to mass measurements.

The mass values from the present measurements are presented in Tables I (Ni), II (Cu), and III (Ga). These tables give the ratio of the cyclotron frequency of the $^{85}\text{Rb}^+$ [40] reference mass to that of the ion of interest. The corresponding uncertainty takes into account a statistical uncertainty depending on the number of ions, and a systematic error [39]. The derived mass excess value is indicated for comparison with the AME tables from 1995 and 2003. Since the latest Atomic-Mass Evaluation (AME2003 [42]) includes the data from this work, the influence of the ISOLTRAP measurements is also provided. Among the 36 nuclides measured here, the influence is 100% for 22 of them.

The nickel results are presented in Table I and in Fig. 2. This figure presents the difference between the mass excess measured by ISOLTRAP and the AME1995 values. Note that even for the stable nickel isotopes the precision of the mass values is improved. With the exception of ^{69}Ni (see below) the results are in good agreement with the 1995 table but much more precise. The masses of $^{57,60,65}\text{Ni}$ agree with the 1995 table within the error bars, and were measured with the same order of uncertainty. The combination of the previous value and the ISOLTRAP measurement reduces the final uncertainty. The results contributing to the ^{69}Ni mass value are presented in Fig. 3. This is a special case because it is in strong disagreement with the AME1995 table [43]: a difference of more than 400 keV was observed. The AME1995 value was derived from a $^{70}\text{Zn}(^{14}\text{C}, ^{15}\text{O})^{69}\text{Ni}$ reaction [44] and a time-of-flight measurement [21]. The ISOLTRAP value disagrees with the value from the reaction but is in agreement with the time-of-flight measurement. Since the value of ISOLTRAP is much more precise, the AME2003 includes only this value.

The copper results are listed in Table II, a comparison with the AME1995 values is given in Fig. 4. An improvement of the mass uncertainty was achieved for all investigated copper isotopes. The values are in good agreement with previous values, except for $^{70}\text{Cu}^n$. This important difference is due to an incorrect state assignment. ISOLTRAP's high resolving power of more than 10^6 , in combination with β -decay studies and selective laser ionization allowed us to perform a clear identification of each state [45]. Moreover, this high resolving power allowed us to resolve isomeric states in ^{68}Cu [46] and to measure them independently. The masses of $^{72-74,76}\text{Cu}$ were previously unknown. They are compared to model predictions in Section IV.

TABLE I: *ISOLTRAP* results for nickel isotopes: nuclide; half life; frequency ratio $\nu_{c,ref}/\nu_c$ of nickel isotope to reference nuclide $^{85}\text{Rb}^+$ [40], corresponding mass excess (ME); mass excess from AME1995; new mass excess from AME2003; influence of the present result on the AME2003 value.

Isotopes	Half life $T_{1/2}$	$\nu_{c,ref}/\nu_c$	ISOLTRAP ME (keV)	AME1995 ME (keV)	AME2003 ME (keV)	Influence on AME2003
^{57}Ni	35.6 h	0.6705736693 (316)	-56084.2 (2.5)	-56075.5 (2.9)	-56082.0 (1.8)	52.0%
^{60}Ni	Stable	0.7057986239 (183)	-64472.7 (1.4)	-64468.1 (1.4)	-64472.1 (0.6)	16.6%
^{64}Ni	Stable	0.7528734602 (163)	-67096.9 (1.3)	-67095.9 (1.4)	-67099.3 (0.6)	21.9%
^{65}Ni	2.5 h	0.7646753441 (285)	-65129.0 (2.3)	-65122.6 (1.5)	-65126.1 (0.6)	7.8%
^{66}Ni	55 h	0.7764412560 (181)	-66006.3 (1.4)	-66028.7 (16.0)	-66006.3 (1.4)	100%
^{67}Ni	21 s	0.7882468785 (362)	-63742.7 (2.9)	-63742.5 (19.1)	-63742.7 (2.9)	100%
^{68}Ni	29 s	0.8000274080 (377)	-63463.8 (3.0)	-63486.0 (16.5)	-63463.8 (3.0)	100%
^{69}Ni	12 s	0.8118484759 (466)	-59978.6 (3.7)	-60380 (140)	-59979 (4)	100%

TABLE II: *ISOLTRAP* results for copper isotopes: nuclide; half life; frequency ratio $\nu_{c,ref}/\nu_c$ of copper isotope to reference nuclide $^{85}\text{Rb}^+$ [40], corresponding mass excess (ME); mass excess from AME1995; new mass excess from AME2003; influence of the present result on the AME2003 value. Previously unknown values derived from systematic trends are marked with #.

Isotopes ^a	Half life $T_{1/2}$	$\nu_{c,ref}/\nu_c$	ISOLTRAP ME (keV)	AME1995 ME (keV)	AME2003 ME (keV)	Influence on AME2003
^{65}Cu	Stable	0.7646483448 (139)	-67264.5 (1.1)	-67259.7 (1.7)	-67263.7 (0.7)	36.8%
^{66}Cu	5.1 m	0.7764380632 (257)	-66258.8 (2.0)	-66254.3 (1.7)	-66258.3 (0.7)	11.1%
^{67}Cu	62 h	0.7882016658 (155)	-67318.8 (1.2)	-67300.2 (8.1)	-67318.8 (1.2)	100%
$^{68}\text{Cu}^g$	31.1 s	0.8000008176 (199)	-65567.0 (1.6)	-65541.9 (45.6)	-65567.0 (1.6)	100%
$^{68}\text{Cu}^m$	3.7 m	0.8000098791 (188)	-64850.3 (1.5)	-64818 (50)	-64845.4 (1.7)	50%
^{69}Cu	2.8 m	0.8117756816 (174)	-65736.2 (1.4)	-65739.9 (8.1)	-65736.2 (1.4)	100%
$^{70}\text{Cu}^g$	45 s	0.8235875816 (199)	-62976.1 (1.6)	-62960.3 (14.5)	-62976.1 (1.6)	100%
$^{70}\text{Cu}^m$	33 s	0.8235888547 (258)	-62875.4 (2.0)	-62859 (15)	-62875.4 (2.0)	100%
$^{70}\text{Cu}^n$	6.6 s	0.8235906419 (272)	-62734.1 (2.1)	-62617 (15)	-62734.1 (2.1)	100%
^{71}Cu	19 s	0.8353679363 (194)	-62711.1 (1.5)	-62764.2 (35.2)	-62711.1 (1.5)	100%
^{72}Cu	6.6 s	0.8471819597 (182)	-59783.0 (1.4)	-60060# (200#)	-59783.0 (1.4)	100%
^{73}Cu	4.2 s	0.8589690332 (491)	-58986.6 (3.9)	-59160# (300#)	-58987 (4)	100%
^{74}Cu	1.6 s	0.8707837184 (779)	-56006.2 (6.2)	-55700# (400#)	-56006 (6)	100%
^{76}Cu	640 ms	0.8944013229 (843)	-50976.0 (6.7)	-50310# (600#)	-50976 (7)	100%

^ag,m,n denote the ground, first excited, and second excited state, respectively, of the nuclide.

The gallium results are presented in Table III and in Fig. 5. The ^{68}Ga mass uncertainty, $\delta m/m \approx 5.4 \cdot 10^{-7}$ is much higher than for all the other nuclides. This is due to the use of a shorter excitation time (100 ms compared to 900 ms for the other nuclides) and to a lack of statistics: only 530 ions were observed, compared to at least 3000 for most of the other ones. The ISOLTRAP value is still in agreement with the AME1995 value but has no influence. For all other gallium isotopes measured by ISOLTRAP the uncertainty was decreased. For five of them, it was decreased by more than a factor of 20, and for ^{63}Ga , almost 100 times.

ence of a 9.5-second isomeric state having an excitation energy of only 60 keV (this accounts for the large AME1995 error bar in Fig. 5). Spectroscopy studies performed in parallel with the mass measurements revealed no indication that the isomer was produced. A two-second excitation time was used in order to resolve this state in the precision trap but it was not seen. Moreover, the z-class analysis [39] was performed to examine any dependence of the result as a function of ion number, but revealed no indication of a contaminant. Therefore we are confident that the present result is that of the ground-state mass.

The case of ^{74}Ga was complicated by the possible pres-

TABLE III: *ISOLTRAP* results for gallium isotopes: nuclide; half life; frequency ratio $\nu_{c,ref}/\nu_c$ of gallium isotope to reference nuclide $^{85}\text{Rb}^+$ [40], corresponding mass excess (ME); mass excess from AME1995; new mass excess from AME2003; influence of the present result on the AME2003 value.

Isotopes	Half life	$\nu_{c,ref}/\nu_c$	ISOLTRAP	AME1995	AME2003	Influence
	$T_{1/2}$		ME (keV)	ME (keV)	ME (keV)	on AME2003
^{63}Ga	32 s	0.7412298391 (167)	-56547.1 (1.3)	-56689.3 (100.0)	-56547.1 (1.3)	100%
^{64}Ga	2.6 m	0.7529779275 (294)	-58834.1 (2.3)	-58834.7 (3.9)	-58834.3 (2.0)	75.2%
^{65}Ga	15 m	0.7647065938 (176)	-62657.3 (1.4)	-62652.9 (1.8)	-62657.2 (0.8)	35.6%
^{68}Ga	68 m	0.799981231 (431)	-67116.2 (34.1)	-67082.9 (2.0)	-67086.1 (1.5)	0%
^{69}Ga	Stable	0.8117302720 (193)	-69327.9 (1.5)	-69320.9 (3.0)	-69327.8 (1.2)	65.3%
^{70}Ga	21 m	0.8235125549 (272)	-68910.3 (2.2)	-68904.7 (3.1)	-68910.1 (1.2)	31.8%
^{71}Ga	Stable	0.8352740255 (357)	-70138.9 (2.8)	-70136.8 (1.8)	-70140.2 (1.0)	13.3%
^{72}Ga	14.1 h	0.8470706093 (182)	-68590.2 (1.4)	-68586.5 (2.0)	-68589.4 (1.0)	53.0%
^{73}Ga	4.8 h	0.8588335898 (208)	-69699.4 (1.7)	-69703.8 (6.3)	-69699.3 (1.7)	100%
^{74}Ga	8.1 m	0.8706314521 (469)	-68049.6 (3.7)	-68054.0 (70.7)	-68050 (4)	100%
^{75}Ga	130 s	0.8824032092 (305)	-68464.6 (2.4)	-68464.2 (6.8)	-68464.6 (2.4)	100%
^{76}Ga	33 s	0.8942076217 (246)	-66296.7 (2.0)	-66202.9 (90.0)	-66296.6 (2.0)	100%
^{77}Ga	13 s	0.9059884728 (303)	-65992.4 (2.4)	-65874.1 (60.0)	-65992.3 (2.4)	100%
^{78}Ga	5.1 s	0.9177943761 (307)	-63706.6 (2.4)	-63662.1 (80.1)	-63706.6 (2.4)	100%

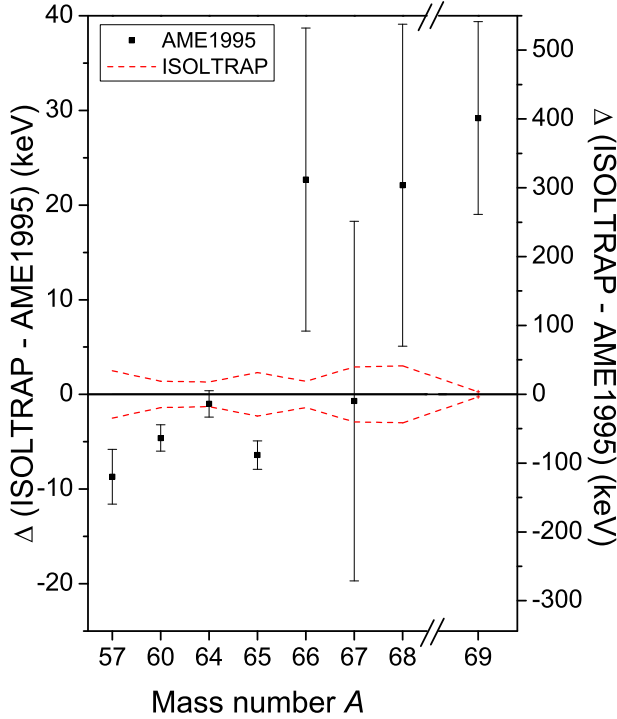


FIG. 2: Difference between the *ISOLTRAP* mass excess results for nickel isotopes and the AME1995 values [43]. Dashed lines represent the *ISOLTRAP* error bars.

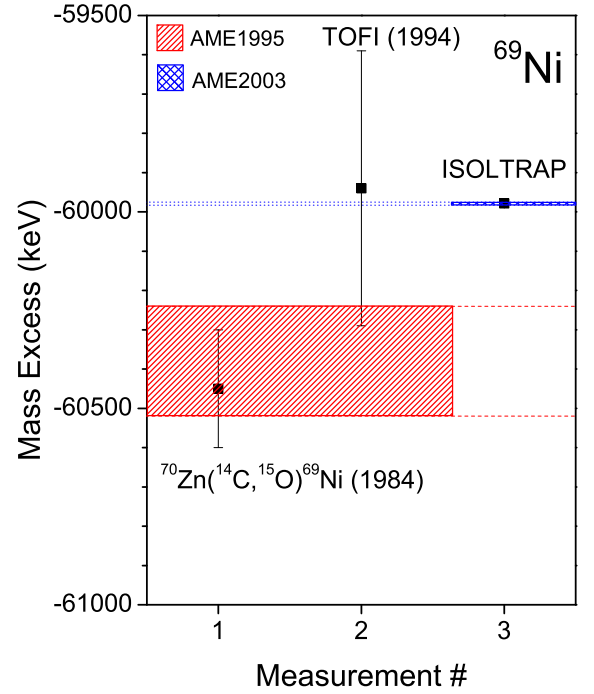


FIG. 3: Mass excess of ^{69}Ni determined by the reaction $^{70}\text{Zn}(^{14}\text{C}, ^{15}\text{O})^{69}\text{Ni}$ [44], and a time-of-flight measurement [21], the resulting AME1995 value [43], and the *ISOLTRAP* value. The AME2003 value [42] differs by 400 keV with an uncertainty 30 times smaller than the AME1995 value.

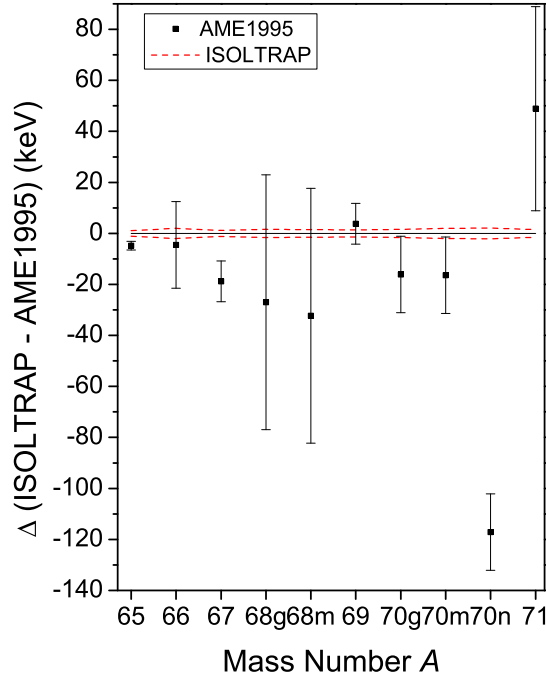


FIG. 4: Difference between *ISOLTRAP* mass-excess values for copper isotopes and the 1995 AME values [43]. Dashed lines represent the *ISOLTRAP* error bars. *g* denotes ground states and *m,n* isomeric states.

IV. MASS-MODEL PREDICTIONS COMPARED WITH NEW DATA

Various models and formulae have been developed over the years to predict properties of nuclides, particularly their mass. A review can be found in [47] where a subset of mass models was singled out for comparison. We have chosen to compare our experimental data to those, as described below.

The venerable Bethe-Weizsäcker mass formula [48, 49], was based on the liquid drop model and did not include shell effects. The nuclear mass m is given by

$$m(N, Z)c^2 = Zm_p c^2 + Nm_n c^2 - a_v A + a_s A^{2/3} + a_c Z^2 A^{-1/3} + a_{sym} \frac{(Z - A/2)^2}{A}, \quad (5)$$

where m_p and m_n are the proton and neutron masses, and A the mass number of the nucleus. The parameters are: a_v the volume term, a_s the surface term, a_c the Coulomb parameter, and a_{sym} the asymmetry parameter. Note that the tabulated masses are those of the neutral atoms, not of the bare atomic nuclei. While inappropriate for mass predictions, it can play an interesting diagnostic role concerning closed shell effects (see section V D).

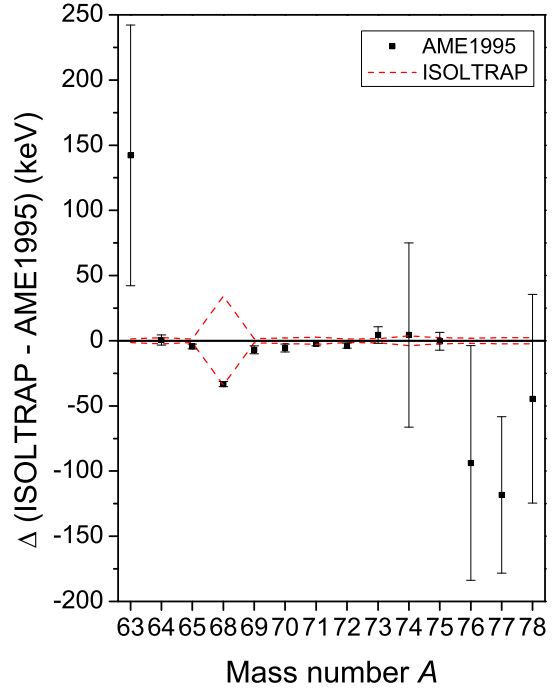


FIG. 5: Difference between *ISOLTRAP* mass-excess values for gallium isotopes and the 1995 AME values [43]. Dashed lines represent the *ISOLTRAP* error bars.

For many years, a hybrid approach was adopted for predicting masses based on a combination of the macroscopic liquid drop model and microscopic (*e.g.* shell) corrections. The most developed form of these so-called mic-mac models is the Finite Range Droplet Model (FRDM) [50].

The Duflo-Zuker (DZ) mass formula [51], is a global approach, derived from a Shell-Model Hamiltonian and gives the best fit to the known masses. Shell-Model calculations, while well-suited for excitation energies, are less so for mass predictions although some efforts were made in this direction [52].

In the last few years, Hartree-Fock Bogolioubov (HFB) calculations have been applied to the construction of complete mass tables. Skyrme forces have traditionally aimed at predicting a wide range of nuclear properties [53, 54, 55, 56]. The first microscopic Skyrme-force mass formula HFBCS-1 [57, 58] was rapidly superseded by HFB-1 [59] which, in turn, was considerably revised, resulting in HFB-2 [60]. A systematic study of the different adjustable parameters followed, resulting in a series of formulas up to HFB-9 [61, 62, 63, 64].

In addition to DZ and FRDM, the *ISOLTRAP* results are therefore compared to HFB-2 and the recent HFB-8 (HFB-9 did not change the mass predictions appreciably).

One characterization of a model is the root-mean-

square (*rms*) deviation from the mass values to which its parameters were fitted, defined by

$$\sigma_{rms} = \frac{1}{N} \sqrt{\sum_{i=1}^N (m_{exp}^i - m_{th}^i)^2}, \quad (6)$$

where N is the number of experimental m_{exp} and theoretical m_{th} masses being compared. A more complete description of the *rms* deviation, including errors, can be found in [47]. Table IV shows σ_{rms} for the models compared with the AME95 table [43], which does not include the present ISOLTRAP results, and with AME03 [42], which does. Our results improved the overall agreement for the HFB models, worsened it for the Duflo-Zuker (DZ) mass formula and for FRDM there is no change. Examining the isotopic chains individually, we see that in all cases the HFB models improved and the DZ model worsened. For the FRDM, the better fit for the gallium isotopes counters the worse fit for copper and nickel. The differences are admittedly small (between 1 and 10%). While it is tempting to conclude that the comparison of the σ_{rms} might be a demonstration of the positive evolution of HFB-2 to HFB-8, it is important to recall that unlike FRDM and DZ, HFB-8 was adjusted to the masses of the AME03.

TABLE IV: The root-mean-square deviation σ_{rms} (in MeV) for different models: the Duflo-Zuker (DZ) mass formula, the Finite Range Droplet Model (FRDM), and the Hartree-Fock Bogolioubov (HFB) calculations, performed with the AME tables of 1995 and 2003 (the latter includes the present ISOLTRAP data). Calculations were made for the nickel, copper, and gallium isotopes measured by ISOLTRAP. The first two rows present the calculation for all nuclides and the following rows describe the results for each isotopic chain separately.

Nuclide	AME Table	DZ	FRDM	HFB-2	HFB-8
Ni,Cu,Ga	AME95	0.434	0.555	0.843	0.550
Ni,Cu,Ga	AME03	0.451	0.555	0.801	0.530
Ni	AME95	0.623	0.445	1.211	0.732
Ni	AME03	0.640	0.476	1.174	0.678
Cu	AME95	0.426	0.471	0.644	0.601
Cu	AME03	0.451	0.530	0.626	0.563
Ga	AME95	0.280	0.644	0.654	0.375
Ga	AME03	0.291	0.614	0.648	0.384

Of particular interest for mass models is to compare predictions as far as possible from what is already known. In the case of the copper isotopes presented here, four new masses were determined and one of them (^{76}Cu) has

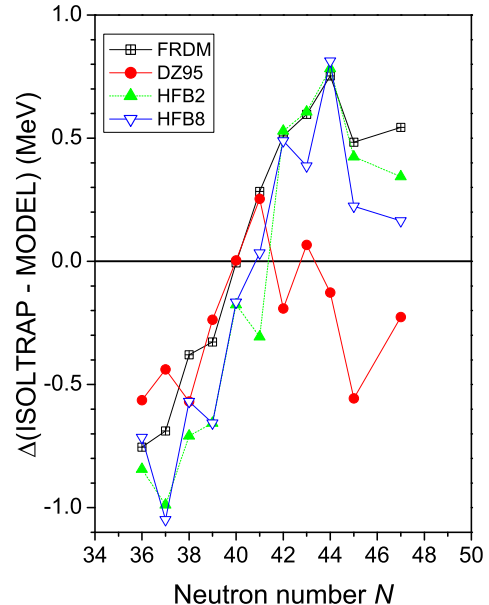


FIG. 6: Mass difference between ISOLTRAP results and model predictions for the copper isotopes. Note that $^{72,73,74,76}\text{Cu}$ are measured for the first time and that the more recent parameter fit for HFB-8 included these results.

five neutrons more than the most neutron-rich previously known mass. The differences of the new ISOLTRAP copper masses with respect to the above-mentioned models are shown in Fig. 6.

Despite going significantly farther from stability, it is difficult to assess which model does a better job. The one closest to the new mass of ^{76}Cu is HFB-8, however the other models are not far away. The *rms* errors on just the four previously unknown masses are also similar with DZ (0.309 MeV) seeming to follow with a better trend compared to all the others (HFB-8: 0.400 MeV; HFB-2: 0.566 MeV; FRDM: 0.603 MeV). It is surprising that despite all models having their parameters adjusted to the mass tables that included those nuclides with $N < 43$, those masses are not very well reproduced locally.

Some nucleon-nucleon effective interactions – like for instance Skyrme SKM*, SLy4, or Gogny D1 – are designed to give rise to a realistic mean field (including pairing). They are therefore parameterized on the ground of a few available nuclear data for which mean field (including pairing) effects can be reasonably disentangle from long range correlations ones (for instance, binding energies of doubly magic nuclei only). Such approaches of nuclei in which long range correlations are not introduced in the mean field in an effective and somewhat uncontrolled manner do not have as objective to give a precise mass formula at the mean (HFB) (including pairing) level, but to constitute the mean field input of more elaborated descriptions of nuclei considering – at least

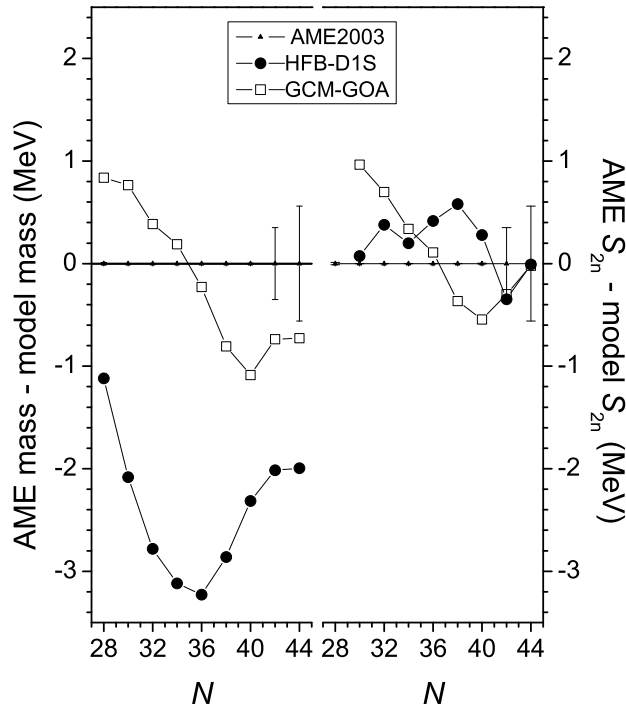


FIG. 7: Difference of the nickel results from the Atomic Mass Evaluation 2003 (AME2003) which already includes the present ISOLTRAP data and those predicted by HFB-D1S (Gogny) and GCM-GOA as a function of neutron number N for (left) the mass and (right) the two-neutron separation energy.

some – long range correlations up to the best and therefore able to describe “beyond” mean field a large class of nuclear observable (mass formula but also low energy spectroscopy, shape coexistence, and transitions, etc ...). In this frame, we have performed triaxial HFB calculations, using numerical methods and codes described in [65], with the Gogny D1S force [66, 67, 68]. Fig. 7 (left) presents the differences between the measured Ni masses and those predicted by HFB-D1S, as a function of N . There is a large offset (rms difference of 2.473 MeV) for the HFB-D1S masses, expected, as explained above, specially for mid-shell nuclei where long range correlations play an important role. Under these assumptions, we could expect at least that the derivative of these quantities might be closer to reality. Therefore, in Fig. 7 (right), we have plotted the two-neutron separation energy S_{2n} [see eq. (7)] derived from the same results. The result is encouraging, with an rms deviation of only 0.508 MeV.

In general, due to the existence of long range correlations beyond mean field, a unique HFB wave function is not well suited to describe the nuclear system. Thus, a configuration mixing approach already described and ap-

plied with some noticeable successes to different nuclear problems, for instance to shape coexistence and transitions in light mercury isotopes [69], or Normal-Superdeformed phenomena [70, 71] has been considered. Using a Generator Coordinate approach under Gaussian Overlap Approximation (GCM-GOA) in a space constituted by HFB (D1S) states under axial and triaxial quadrupole constraints allows in this model to treat on the same footing rotation and quadrupole vibrations. This approach which takes explicitly into account these important correlations, has been applied to the calculation of nickel masses, and the results are shown in Fig. 7 for comparison. Already the mass values (left) are greatly improved (rms difference of 0.701 MeV), as are the mass derivatives (right, rms difference of 0.335 MeV). It would appear that going beyond the mean field is to be encouraged for future mass predictions. Works in this spirit are also underway on the ground of Skyrme forces (see *e.g.* [72]).

V. ANALYSIS OF THE MASS SURFACE AROUND $Z=29$ AND $N=40$

As recalled in the introduction, Bohr and Mottelson [20] explain that the effects of binding energy on nuclear structure are subtle but decisive. As such, accurate mass measurements are important in order to finely analyse the mass surface, notably its derivatives. In this section we examine several mass-surface derivatives and variations.

A. Study of the two-neutron separation energy

The two-neutron separation energy (S_{2n}) given by

$$S_{2n}(N, Z) = B(N, Z) - B(N - 2, Z), \quad (7)$$

with B for the binding energy, is remarkable for its regularity between shell closures. Generally, S_{2n} decreases smoothly with N and shell effects appear as discontinuities. In the past, discontinuities of S_{2n} versus N were often traced to inaccurate Q_β endpoint measurements and measurements with more reliable, direct techniques restored the regularity (see, for example, [73] for the area around ^{208}Pb). Hence, part of the motivation was to confirm any mass surface irregularities in the $N = 40$ region. Fig. 8 presents the S_{2n} values, from $N = 36$ to 50, prior and after the ISOLTRAP mass measurements. Most of the irregularities *e.g.* at $N = 41$ for gallium are confirmed. Moreover, the plot reveals a deviation from the linear trend between $N = 39$ and $N = 41$ for nickel, copper, and gallium. Also irregularities for gallium ($N = 46 - 49$) and copper ($N = 43 - 46$) are visible.

To study the structure more closely we subtract a linear function of N determined by the S_{2n} slope preceding the purported shell closure. The resulting reduced S_{2n} values are presented in Fig. 9 in the region of $N = 82$ (for comparison) and $N = 40$. The $N = 82$ shell closure

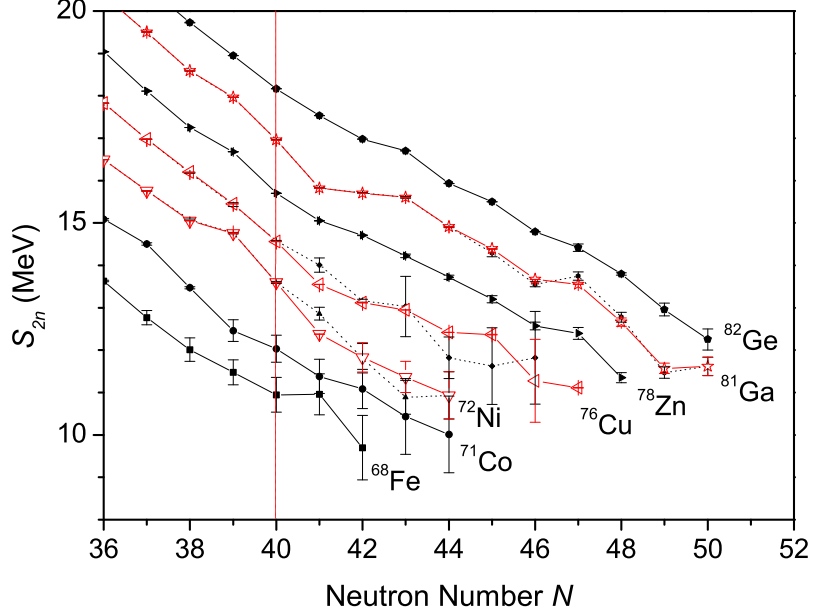


FIG. 8: Two-neutron separation energies (S_{2n}) for iron ($Z = 26$) to germanium ($Z = 32$) around $N = 40$. Dashed lines correspond to the data before the ISOLTRAP measurements. Points with large error bars were not directly measured by ISOLTRAP but their value was changed by the link to the measured masses.

is clearly visible on this plot: there is a change of slope between $N = 82$ and $N = 84$. From these observations we can analyse the behavior in the $N = 40$ region: there is a similar effect between $N = 39$ and $N = 41$ where the break can be seen at $N = 39$ and not at $N = 40$, surprising for an odd number. The magnitude of this decrease is far smaller (between 500 keV and 1 MeV) than the one for the major shell closure at $N = 82$ (around 4 MeV). A similar structure is seen between $N = 39$ and $N = 41$ for nickel, copper, and gallium, but this is not an indication of shell closure. It is strange that the same structure is visible for both nickel (even Z) and gallium (odd Z) whereas germanium is smooth and little is seen in the case of zinc. Further measurements to reduce the uncertainty on the neighboring cobalt isotopes will be needed.

B. The shell gap

The neutron shell gap, defined as

$$\begin{aligned} \Delta_N(N, Z) &= S_{2n}(N, Z) - S_{2n}(N + 2, Z) \\ &= 2B(N, Z) - B(N - 2, Z) - B(N + 2, Z), \end{aligned} \quad (8)$$

is a good indicator of shell strength. The shell gap definition is usually only valid for spherical nuclides, *i.e.* around magic numbers. Here, we examine the case of

$N = 40$ and also investigate how mid-shell gaps compare in strength and comportment. Fig. 10, calculated from AME2003 data [42], shows the shell gap as a function of the proton number Z for various N . This highlights the large shell gap values for magic neutron number with peaks at magic Z . It also shows that for $N = 50$ there is a peak at $Z = 39$, and not $Z = 40$, which is known to be semi-magic. This behavior is probably due to the odd-even effect in the two-proton separation energy S_{2p} . Not surprisingly, the mid-shell-gap ($N = 39, 66$) energies are quite small. From this point of view, the case of $N = 40$ resembles a mid-shell rather than a magic number.

Fig. 11 shows the details of adjacent shell gaps Δ_N as a function of the proton number Z for different regions: (a) around a shell closure, (b) in the region of interest, and (c) in a mid-shell region. In Fig. 11(a), the behavior of a strong shell closure is shown for $N = 82$ which is a magic number: there is a large difference between $N = 82$ and $N = 81, 83$ and the corresponding enhanced shell gap for the case of magic $Z = 50$. Fig. 11(c) shows the behavior of the mid-shell region around $N = 66$ (exactly in between two shell closures: 50 and 82): the neutron shell gap for $N = 66$ is between the one for $N = 65$ and $N = 67$. Fig. 11(b) presents the shell gap around $N = 40$. For $N = 40$ a strong difference (like for $N = 82$) is not visible and $N = 40$ is distinct from neither $N = 39$ nor 41. Note that the $N = 39$ mid-shell gap is larger than those of $N = 38$ and 40 for several values of Z , especially

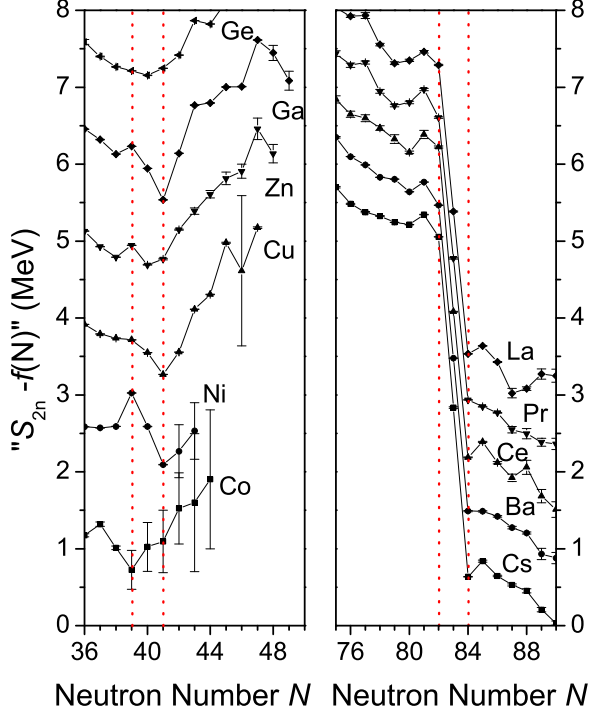


FIG. 9: Two-neutron separation energies (S_{2n}) minus a linear function of N around $N = 40$ (left), and the strong shell closure $N = 82$ (right), for comparison.

for $Z = 28$, unlike the $N = 66$ mid-shell behavior. This shows that $N = 38, 39$, and 40 do not have the behavior we could have expected from observation in other mass regions. However, in summary, no shell closure at $N = 40$ is observed.

C. The pairing gap

The pairing gap from the four-point formula [74] $\Delta_4(N, Z)$

$$\Delta_4(N, Z) = \frac{(-1)^N}{4} \left(B(N+1) - 3B(N) + 3B(N-1) - B(N-2) \right) \quad (9)$$

was chosen to study the pairing-energy behavior. A peak is expected for magic numbers and a trough at mid-shell.

The pairing gap as a function of neutron number is presented in Fig. 12(a) for $Z = 28 - 32$. At the $N = 39$ mid-shell, there is a trough for $Z = 31$ - but not for $Z = 29$. A similar behavior is seen at $N = 66$ ($82-50$ mid-shell). The odd- Z nuclides have a lower pairing gap and while germanium ($Z = 32$) shows no particular structure, nickel ($Z = 28$) shows a strong mid-shell trough and not

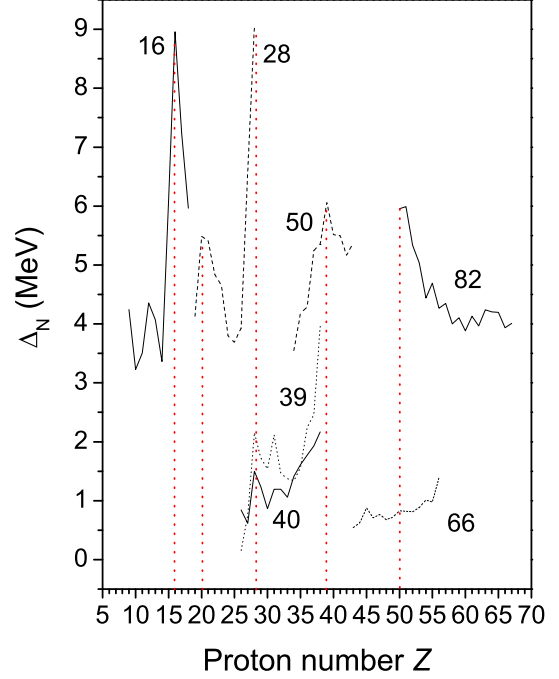


FIG. 10: (a) Shell gap as a function of the proton number Z for different magic and mid-shell neutron numbers N . $N=16, 28, 50, 82$ correspond to shell closures, $N = 39$ and 66 are exactly between two shell closures (called mid-shell), $N = 40$ is under investigation. Data are from [42].

a peak that would indicate a shell closure, as shown in Fig. 12(b) where shell closure at $N = 28, 50$, and 82 are clearly visible.

D. Comparison with the Bethe-Weizsäcker formula

The Bethe-Weizsäcker formula was given in eq. (5). We adapt the version of Pearson [75], with a pairing term of Fletcher [76]. Thus, the binding energy per nucleon is given by

$$\begin{aligned} \frac{E_{nuc}}{A} = & a_{vol} + a_{sf}A^{-1/3} + \frac{3e^2}{5r_0}Z^2A^{-4/3} \\ & + (a_{sym} + a_{ss}A^{-1/3})I^2 \\ & + a_pA^{-y-1} \left(\frac{(-1)^Z + (-1)^N}{2} \right), \end{aligned} \quad (10)$$

with $I = (N - Z)/A$. The parameters are $a_{vol} = -15.65$ MeV, $a_{sf} = 17.63$ MeV, $a_{ss} = -25.60$ MeV which is the parameter of surface symmetry term introduced by Myers and Swiatecki [77], $a_{sym} = 27.72$ MeV, $r_0 = 1.233$ fm with r_0 the constant used in the radius estimation $R \approx r_0A^{1/3}$, $a_p = -7$ MeV the pairing term,

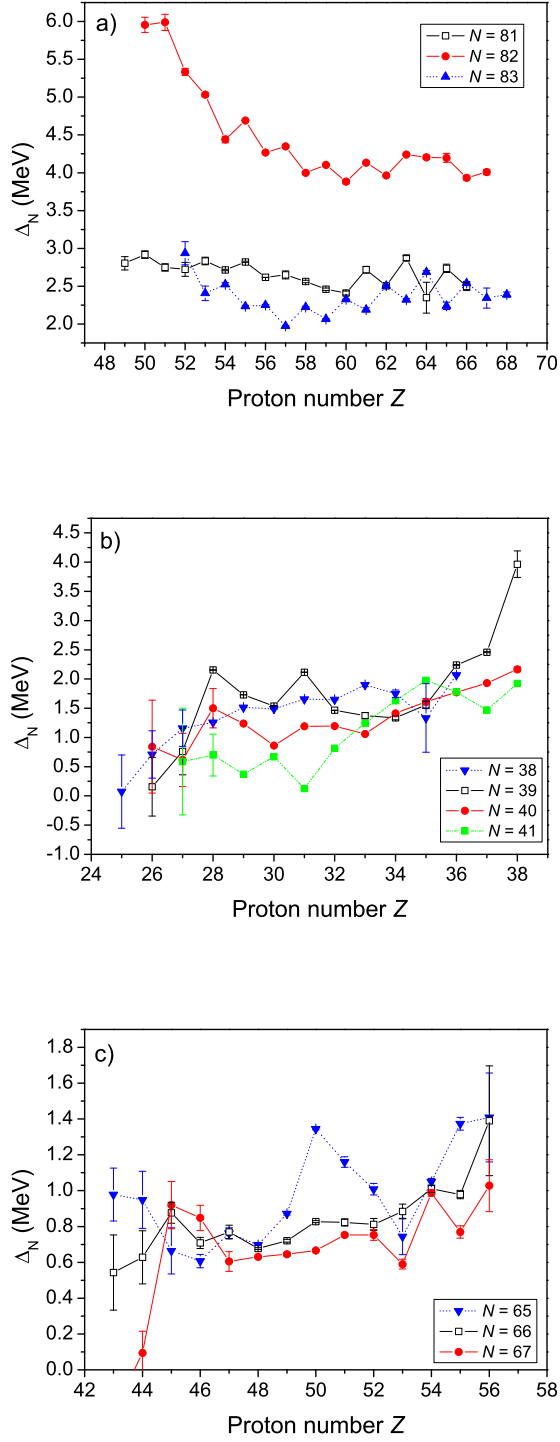


FIG. 11: Shell gap as a function of the proton number Z for a) $N = 81 - 83$ with the $N=82$ magic number well distinguished from $N=81$ and 83 , b) $N = 38 - 41$, and c) $N = 65 - 67$ with $N=66$ representing a mid-shell number in between $N=50$ and 82 .

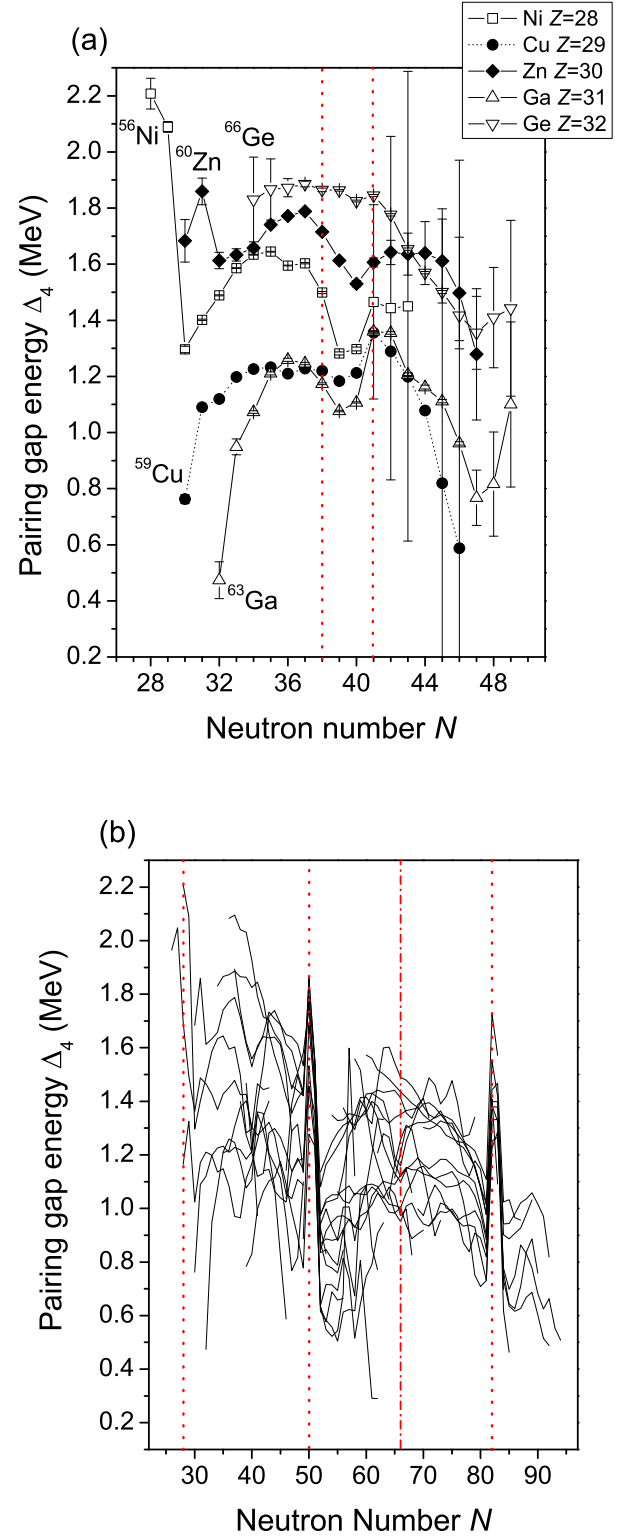


FIG. 12: (a) Pairing gap energy as a function of neutron number for the investigated elements: nickel, copper, and gallium, as well as zinc and germanium. (b) Pairing gap energy as a function of neutron number for $Z=27-59$. Shell closures at $N=28, 50$, and 82 are clearly visible, the $N=66$ mid-shell is indicated.

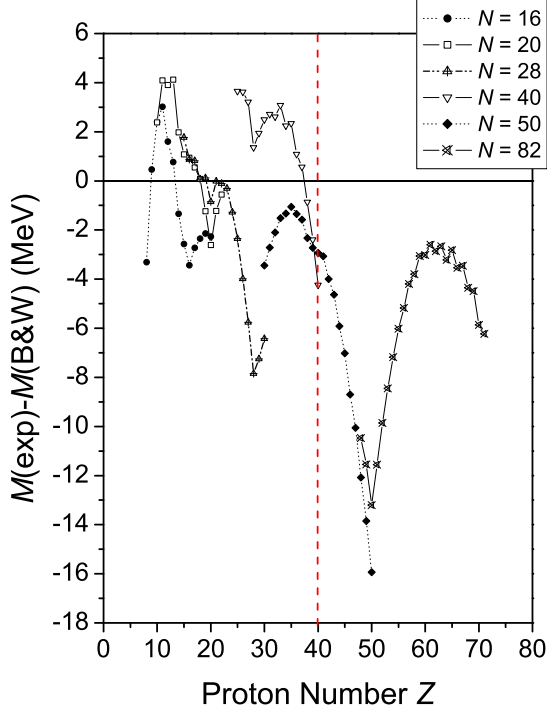


FIG. 13: Difference between the experimental mass values from this work and from AME2003 data [42] and theoretical masses from the “Bethe-Weizsäcker formula” as a function of proton number, for several magic neutron numbers and for $N=40$.

and $y = 0.4$. This formula contains no specific term for shell effects so the formula may not be a good way to predict exotic mass values. However this makes it a “neutral” indicator for shell structures (see [78]).

To this end, the modified Weizsäcker formula [eq. (10)] is subtracted from known masses (divided by A). The difference between the experimental values and the formula clearly reveals the shell closures at $N = 28, 50, 82$ and 126 , reaching up to 15 MeV for $N = 50$ and $N = 82$ (see Fig. 1 in [75]).

Fig. 13 presents the difference between the experimental results obtained from this work (complemented with AME2003 data) with the “Bethe-Weizsäcker formula” [eq. (10)] as a function of Z for various magic neutron numbers, including $N = 40$. As with the shell gaps, the cases where $N = Z$ show the strongest effects, as does the case of $^{132}_{50}\text{Sn}_{82}$. Interestingly enough, the case of $^{68}_{28}\text{Ni}_{40}$ does show a dip of about 2 MeV, although only about 20% the effect of $^{132}_{50}\text{Sn}_{82}$.

When the difference in mass values is examined isotopically as a function of neutron number (Fig. 14), however, there is no indication of a shell, or even sub-shell closure. The pseudo-parabolic behavior of the curve in Fig. 14 shows some indentation around $N = 40$ but nothing

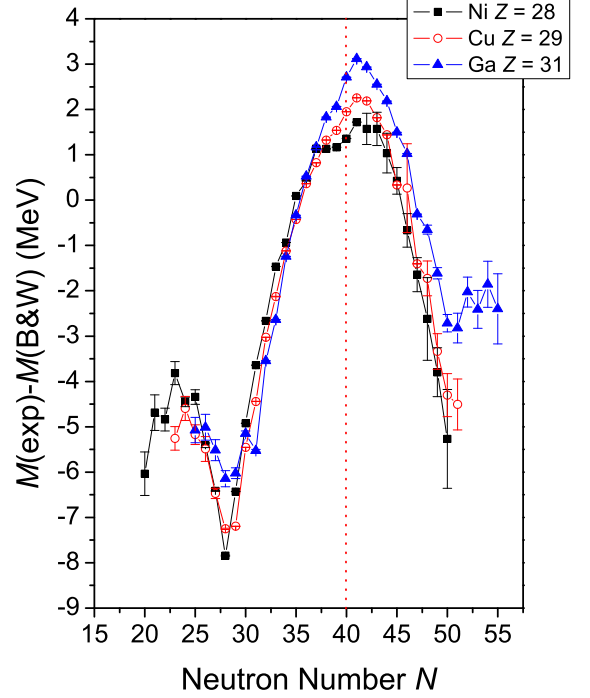


FIG. 14: Difference between the masses predicted by the Bethe-Weizsäcker formula (eq. 10) and the experimental values as a function of N for $Z = 28, 29$, and 31 . Data are from this work complemented by [42].

ing that we could claim to be “magic”.

VI. CONCLUSION

The high-precision mass measurements performed at ISOLTRAP on over 30 short-lived neutron-rich isotopes of nickel, copper, and gallium have allowed us to rather finely study the mass surface – and its derivatives – around the interesting region of $Z = 28$ and $N = 40$. No behavior resembling that of known magic numbers has been found, unlike the analog case of $Z = 40$, where the $N = 56$ sub-shell closure is visible. As much as an $N = 40$ ($d_{5/2}$) sub-shell could exist, there is no clear indication for such a sub-shell closure from these measurements. While the pairing gap energy clearly indicates that there is no shell closure in this region, a competing mid-shell stabilization effect might be present. The comparison with the Bethe-Weizsäcker formula shows some fine structure around $N = 39, 40$ but no indication of the presence of a shell, or sub-shell closure. The shell gap evaluation shows anomalous behavior for $N = 39$ as well as for $N = 40$, perhaps due again to the competition between a sub-shell closure at 40 and the mid-shell at 39 .

Recalling again the words of Bohr and Mottelson, “it

is relatively difficult to discern the nuclear shell structure as long as the main information on nuclei is confined to binding energies". While they are a necessary ingredient, it is not sufficient for explaining the problem at hand since the binding energies are in opposition with results on the $B(E2)$ [16]. Thus, more detailed spectroscopy measurements, including the g -factor, as suggested by Langanke *et al.* [19], and more theoretical work, are called for to understand the various phenomena arising from mass-surface studies.

Acknowledgments

The authors thank the ISOLDE technical group for their assistance and acknowledge the GDR *Noyaux Exo-*

tiques. This work was supported by the German Federal Ministry for Education and Research (BMBF) under contract no. 06GF151, by the Helmholtz Association of National Research Centers (HGF) under contract no. VH-NG-037, by the European Commission under contract no. HPRI-CT-2001-50034 (NIPNET), by the ISOLDE Collaboration, by the Marie Curie fellowship network HPMT-CT-2000-00197, and by the French IN2P3.

-
- [1] C. Thibault, R. Klapisch, C. Rigaud, A.M. Poskanzer, R. Prieels, L. Lessard, and W. Reisdorf, Phys. Rev. C **12**, 644 (1975).
 - [2] D. Guillemaud-Mueller, C. Detraz, M. Langevin, F. Naulin, M. De Saint-Simaon, C. Thibault, F. Touchard, and M. Epherre, Nucl. Phys. A **426**, 37 (1984).
 - [3] A. Ozawa, T. Kobayashi, T. Suzuki, K. Yoshida, and I. Tanihata, Phys. Rev. Lett. **84**, 5493 (2000).
 - [4] S. Shimoura, A. Saito, T. Minemura, Y.U. Matsuyama, H. Baba, H. Akiyoshi, N. Aoi, T. Gomi, Y. Higurashi, K. Ieki, et al., Phys. Lett. B **560**, 31 (2003).
 - [5] F. Sarazin, H. Savajols, W. Mittig, F. Nowacki, N.A. Orr, Z. Ren, P. Roussel-Chomaz, G. Auger, D. Baiborodin, A.V. Belozorov, et al., Phys. Rev. Lett. **84**, 5062 (2000).
 - [6] K. Minamisono, P.F. Mantica, T.J. Mertzimekis, A.D. Davies, M. Hass, J. Pereira, J.S. Pinter, W.F. Rogers, J.B. Stoker, B.E. Tomlin, et al., Phys. Rev. Lett. **96**, 102501 (2006).
 - [7] J.I. Prisciandaro, P.F. Mantica, B.A. Brown, D.W. Anthony, M.W. Cooper, A. Garcia, D.E. Groh, A. Komives, W. Kumarasiri, P.A. Lofy, et al., Phys. Lett. B **510**, 17 (2001).
 - [8] P.F. Mantica, B.A. Brown, A.D. Davies, T. Glasmacher, D.E. Groh, M. Horoi, S.N. Liddick, D.J. Morrissey, A.C. Morton, W.F. Mueller, et al., Phys. Rev. C **67**, 014311 (2003).
 - [9] P.F. Mantica, A.C. Morton, B.A. Brown, A.D. Davies, T. Glasmacher, D.E. Groh, S.N. Liddick, D.J. Morrissey, W.F. Mueller, H. Schatz, et al., Phys. Rev. C **68**, 044311 (2003).
 - [10] M. Bernas, P. Dessagne, M. Langevin, J. Payet, F. Pougheon, and P. Roussel, Phys. Lett. B **113**, 279 (1982).
 - [11] L.P. Ekstrom and J. Lyttkens-Linden, Nucl. Data Sheets **67**, 579 (1992).
 - [12] R. Broda, B. Fornal, W. Krölas, T. Pawlat, D. Bazzacco, S. Lunardi, C. Rossi-Alvarez, R. Menegazzo, G. de Angelis, P. Bednarczyk, et al., Phys. Rev. Lett. **74**, 868 (1995).
 - [13] R. Grzywacz, R. Béraud, C. Borcea, A. Emsallem, M. Glogowski, H. Grawe, D. Guillemaud-Mueller, M. Hjorth-Jensen, M. Houry, M. Lewitowicz, et al., Phys. Rev. Lett. **81**, 766 (1998).
 - [14] M. Hannawald, T. Kautzsch, A. Wöhr, W.B. Walters, K.-L. Kratz, V.N. Fedoseyev, V.I. Mishin, W. Böhmer, B. Pfeiffer, V. Sebastian, et al., Phys. Rev. Lett. **82**, 1391 (1999).
 - [15] W.F. Mueller, B. Bruyneel, S. Franchoo, H. Grawe, M. Huyse, U. Köster, K.-L. Kratz, K. Kruglov, Y. Kudryavtsev, B. Pfeiffer, et al., Phys. Rev. Lett. **83**, 3613 (1999).
 - [16] O. Sorlin, S. Leenhardt, C. Donzau, J. Duprat, F. Azaiez, F. Nowacki, H. Grawe, Z. Dombrádi, F. Amorini, A. Astier, et al., Phys. Rev. Lett. **88**, 092501 (2002).
 - [17] O. Perru, O. Sorlin, S. Franchoo, F. Azaiez, E. Bouchez, C. Bourgeois, A. Chatillon, J.M. Daugas, Z. Dlouhy, Z. Dombrádi, et al., Phys. Rev. Lett. **96**, 232501 (2006).
 - [18] I. Stefanescu, G. Georgiev, F. Ames, J. Äystö, D.L. Balabanski, G. Bollen, P.A. Butler, J. Cederkäll, N. Champaault, T. Davinson, et al., submitted to Phys. Rev. Lett. (2006).
 - [19] K. Langanke, J. Terasaki, F. Nowacki, D. J. Dean, and W. Nazarewicz, Phys. Rev. C **67**, 044314 (2003).
 - [20] A. Bohr and B.R. Mottelson, *Nuclear structure*, W.A. BENJAMIN, INC. New York, Amsterdam, Chapter2, Section2 p. 189 (1969).
 - [21] H.L. Seifert, J.M. Wouters, D.J. Vieira, H. Wollnik, X.G. Zhou, X.L. Tu, Z.Y. Zhou, and G.W. Butler, Z. Phys. A **349**, 25 (1994).
 - [22] K. Blaum, Phys. Rep. **425**, 1 (2006).
 - [23] L. Schweikard and G. Bollen (ed.), Int. J. Mass Spectrom. **251(2/3)** (2006).
 - [24] G. Bollen, P. Dabkiewicz, P. Egelhof, T. Hilberath, H. Kalinowsky, F. Kern, H.-J. Kluge, R.B. Moore, H. Schnatz, L. Schweikhard, et al., J. Appl. Phys. **68**, 4355 (1990).
 - [25] H. Stolzenberg, S. Becker, G. Bollen, F. Kern, H.-J. Kluge, T. Otto, G. Savard, L. Schweikhard, G. Audi, and R.B. Moore, Phys. Rev. Lett. **65**, 3104 (1990).
 - [26] E. Kugler, Hyp. Int. **129**, 23 (2000).
 - [27] F. Herfurth, J. Dilling, A. Kellerbauer, G. Bollen, S. Henry, H.-J. Kluge, E. Lamour, D. Lunney, R.B. Moore, C. Scheidenberger, et al., Nucl. Instrum. Methods

- A **469**, 254 (2001).
- [28] H. Raimbault-Hartmann, D. Beck, G. Bollen, M. König, H.-J. Kluge, E. Scharf, J. Stein, S. Schwarz, and J. Szerypo, Nucl. Instrum. Methods B **126**, 378 (1997).
 - [29] G. Savard, S. Becker, G. Bollen, H.-J. Kluge, R.B. Moore, T. Otto, L. Schweikhard, H. Stolzenberg, and U. Wiess, Phys. Lett. A **158**, 247 (1991).
 - [30] L.S. Brown and G. Gabrielse, Rev. Mod. Phys. **58**, 233 (1986).
 - [31] M. König, G. Bollen, H.-J. Kluge, T. Otto, and J. Szerypo, Int. J. Mass Spectrom. Ion Proc. **142**, 95 (1995).
 - [32] K. Blaum, G. Bollen, F. Herfurth, A. Kellerbauer, H.-J. Kluge, M. Kuckein, S. Heinz, P. Schmidt, and L. Schweikhard, J. Phys. B **36**, 921 (2003).
 - [33] G. Bollen, H. Hartmann, H.-J. Kluge, M. König, T. Otto, G. Savard, and H. Stolzenberg, Phys. Scripta **46**, 581 (1992).
 - [34] G. Bollen, S. Becker, H.-J. Kluge, M. König, R.B. Moore, T. Otto, H. Raimbault-Hartmann, G. Savard, L. Schweikhard, H. Stolzenberg, et al., Nucl. Instrum. Meth A **368**, 675 (1996).
 - [35] C. Yazdijian, K. Blaum, R. Ferrer, F. Herfurth, A. Hertler, and L. Schweikhard, Hyp. Int. (to be published).
 - [36] G. Gräff, H. Kalinowsky, and J. Traut, Z. Phys. A **297**, 35 (1980).
 - [37] A. Kellerbauer, Int. J. Mass Spectrom. **229**, 107 (2003).
 - [38] U. Köster, Nucl. Phys. A **701**, 441c (2002).
 - [39] A. Kellerbauer, K. Blaum, G. Bollen, F. Herfurth, H.-J. Kluge, M. Kuckein, E. Sauvan, C. Scheidenberger, and L. Schweikhard, Eur. Phys. J. D **22**, 53 (2003).
 - [40] M.P. Bradley, J.V. Porto, S. Rainville, J.K. Thompson, and D.E. Pritchard, Phys. Rev. Lett. **83**, 4510 (1999).
 - [41] A.H. Wapstra, G. Audi, and C. Thibault, Nucl. Phys. A **729**, 129 (2003).
 - [42] G. Audi, A.H. Wapstra, and C. Thibault, Nucl. Phys. A **729**, 337 (2003).
 - [43] G. Audi and A.H. Wapstra, Nucl. Phys. A **595**, 409 (1995).
 - [44] Ph. Dessagne, M. Bernas, M. Langevin, G.C. Morrison, J. Payet, F. Pougheon, and P. Roussel, Nucl. Phys. A **426**, 399 (1984).
 - [45] J. Van Roosbroeck, C. Guénaut, G. Audi, D. Beck, K. Blaum, G. Bollen, J. Cederkall, P. Delahaye, H. De Witte, D. Fedorov, et al., Phys. Rev. Lett. **92**, 112501 (2004).
 - [46] K. Blaum, D. Beck, G. Bollen, P. Delahaye, C. Guénaut, F. Herfurth, A. Kellerbauer, H.-J. Kluge, D. Lunney, S. Schwarz, et al., Europhys. Lett. **67**, 586 (2004).
 - [47] D. Lunney, J.M. Pearson, and C. Thibault, Rev. Mod. Phys. **75**, 1021 (2003).
 - [48] C.F. von Weizsäcker, Z. Phys. **96**, 431 (1935).
 - [49] H.A. Bethe and R.F. Bacher, Rev. Mod. Phys. **8**, 82 (1936).
 - [50] P. Möller, J.R. Nix, W.D. Myers, and W.J. Swiatecki, At. Data Nucl. Data Tables **59**, 185 (1995).
 - [51] J. Duflo and A.P. Zuker, Phys. Rev. C **59**, R2347 (1999).
 - [52] E. Caurier, G. Martínez-Pinedo, F. Nowacki, A. Poves, J. Retamosa, and A.P. Zuker, Rev. Mod. Phys. **77**, 427 (2005).
 - [53] H. Flocard, S.E. Koonin, and M.S. Weiss, Phys. Rev. C **17**, 1682 (1978).
 - [54] P. Bonche, J. Dobaczewski, H. Flocard, P.-H. Heenen, and J. Meyer, Nucl. Phys. A **510**, 466 (1990).
 - [55] P.-H. Heenen, P. Bonche, and H. Flocard, Nucl. Phys. A **588**, 490 (1995).
 - [56] P. Bonche, H. Flocard, and P.-H. Heenen, Comp. Phys. Com. p. In press (2005).
 - [57] F. Tondeur, S. Goriely, J.M. Pearson, and M. Onsi, Phys. Rev. C **62**, 024308 (2000).
 - [58] S. Goriely, F. Tondeur, and J.M. Pearson, At. Data Nucl. Data Tables **77**, 311 (2001).
 - [59] M. Samyn, S. Goriely, P.-H. Heenen, J.M. Pearson, and F. Tondeur, Nucl. Phys. A **700**, 142 (2001).
 - [60] S. Goriely, M. Samyn, P.-H. Heenen, J.M. Pearson, and F. Tondeur, Phys. Rev. C **66**, 024326 (2002).
 - [61] M. Samyn, S. Goriely, and J.M. Pearson, Nucl. Phys. A **725**, 69 (2003).
 - [62] S. Goriely, M. Samyn, M. Bender, and J.M. Pearson, Phys. Rev. C **68**, 054325 (2003).
 - [63] M. Samyn, S. Goriely, M. Bender, and J.M. Pearson, Phys. Rev. C **70**, 044309 (2004).
 - [64] S. Goriely, M. Samyn, J.M. Pearson, and M. Onsi, Nucl. Phys. A **750**, 425 (2005).
 - [65] M. Girod and B. Grammaticos, Phys. Rev. C **27**, 2317 (1983).
 - [66] J. Dechargé and D. Gogny, Phys. Rev. C **21**, 1568 (1980).
 - [67] J.F. Berger, M. Girod, and D. Gogny, Comput. Phys. Commun. **63**, 107 (1991).
 - [68] D. Gogny, in *Proceedings of the International Conference on Nuclear Physics, Munich, 1973*, edited by J. De Boer and H.J. Mang (North Holland, Amsterdam, 1973); in *Proceedings of the International Conference on Nuclear Selfconsistent fields, Trieste, 1975*, edited by G. Ripka and M. Porneuf (North Holland, Amsterdam, 1975).
 - [69] J.P. Delaroche, M. Girod, G. Bastin, I. Deloncle, F. Hannachi, J. Libert, M.G. Porquet, C. Bourgeois, D. Hojman, P. Kilcher, et al., Phys. Rev. C **50**, 2332 (1994).
 - [70] J. Libert, M. Girod, and J.-P. Delaroche, Phys. Rev. C **60**, 054301 (1999).
 - [71] J.P. Delaroche, M. Girod, H. Goutte, and J. Libert, Nucl. Phys. A **771**, 103 (2006).
 - [72] M. Bender, G.F. Bertsch, and P.-H. Heenen, Phys. Rev. Lett. **94**, 102503 (2005).
 - [73] S. Schwarz, F. Ames, G. Audi, D. Beck, G. Bollen, C. D. Coster, J. Dilling, O. Engels, R. Fossion, J.-E. G. Ramos, et al., Nucl. Phys. A **693**, 533 (2001).
 - [74] J. Bardeen, L.N. Cooper, and J.R. Schrieffer, Phys. Rev. **108**, 1175 (1957).
 - [75] J.M. Pearson, Hyp. Int. **132**, 59 (2001).
 - [76] J.M. Fletcher, Masters thesis, University of Surrey (2003).
 - [77] W.D. Myers and W.J. Swiatecki, Nucl. Phys. **81**, 1 (1966).
 - [78] C. Guénaut, G. Audi, D. Beck, K. Blaum, G. Bollen, P. Delahaye, F. Herfurth, A. Kellerbauer, H.-J. Kluge, D. Lunney, et al., Eur. Phys. J. A Direct **25**, s1.33 (2005).